Molecular Structure and Magnetic Properties of μ-Dihydroxo-bis[2,6-pyridinedicarboxylatoaquoiron(III)] and μ-Dihydroxo-bis[4-hydroxo-2,6-pyridinedicarboxylato-aquoiron(III)] Tetrahydrate

John A. Thich, Chia Chih Ou, Dana Powers, Byron Vasiliou, Donald Mastropaolo, Joseph A. Potenza.*[1,2] and Harvey J. Schugar*[1]

Contribution from the School of Chemistry, Rutgers University, New Brunswick, New Jersey 08903. *Received January 22, 1975*

Abstract: The crystal and molecular structures of the title complexes have been determined from single-crystal three-dimensional x-ray data collected by counter methods. $[Dipic(H_2O)FeOH]_2$ (Dipic or Dipicolinate = 2,6-pyridinedicarboxylate) crystallizes as green prisms in space group $P\bar{1}$ (C_i^1, No. 2): with $Z = 1$; $a = 8.844$ (4), $b = 11.001$ (5), $c = 7.303$ (4) Å; $\alpha = 94.06$ (4), $\beta = 111.56$ (10), $\gamma = 131.54$ (4)°; $d_{calcd} = 1.927$, $d_{obsd} = 1.93$ (1) g/cm^3. Least-squares refinement of 1436 reflections having $F^2 \geq 3\sigma$ gave a conventional R factor of 0.052. The structure consists of centrosymmetric dimeric units in which crystallographically equivalent Fe(III) ions are bridged by two hydroxyl groups. The planar $[Fe_2(OH)_2]^{4+}$ unit has Fe-OH-Fe bridging angles of 103.6 (2)° and a Fe···Fe separation of 3.089 (2) Å. Nonequivalent Fe-OH distances of 1.938 (5) and 1.993 (5) Å reflect the trans influences of the ring N atom and of the coordinated H_2O molecule, respectively. The distorted octahedral coordination geometry of the iron ions is completed by a water molecule and two carboxylate atoms from the tridentate Dipiç ligand. $[Chel(H_2O)FeOH]_2 \cdot 4H_2O$ (Chel or chelidamate = 4-hydroxo-2,6-pyridinedicarboxylate) also crystallizes as green prisms in space group $P\bar{1}$ (C_i^1, No. 2): with $Z = 1$; $a = 7.972$ (4), $b = 11.106$ (4), $c = 7.051$ (3) Å; $\alpha = 67.71$ (3), $\beta = 112.73$ (3), $\gamma = 95.81$ (4)°; $d_{calcd} = 1.923$, $d_{obsd} = 1.92$ (1) g/cm^3. Least-squares refinement of 1543 reflections having $F^2 \geq 3\sigma$ gave a conventional R factor of 0.044. The structural parameters of $[Chel(H_2O)FeOH]_2 \cdot 4H_2O$ are nearly identical with those of $[Dipic(H_2O)FeOH]_2$; the only significant difference between the valence polyhedra is the slight shortening of the Fe···Fe separation from 3.089 (2) Å in the Dipic structure to 3.078 (2) Å in the Chel structure. In both structures, dimers are linked by hydrogen bonds, although the hydrogen bonding network is more extensive in $[Chel(H_2O)FeOH]_2 \cdot 4H_2O$. The magnetic susceptibilities of $[Dipic(H_2O)FeOH]_2$ and $[Chel(H_2O)FeOH]_2 \cdot 4H_2O$ have been measured over the 85–300 K range. In the context of the $H = -2J\bar{S}_1 \cdot \bar{S}_2$ spin–spin coupling model, the susceptibility data can be fit by respective J values of -11.4 (4) and -7.3 (4) cm^{-1} ($\bar{S}_1 = \bar{S}_2 = 5/2$, $g = 2.00$, TIP = 0). The observed extent of antiferromagnetism is discussed in terms of structural and electronic effects. A review of the magnetic properties attributed to the parent Fe(III) aquo dimer $[(H_2O)_4FeOH]_2^{4+}$ is based on those observations.

The phenomenon of reduced paramagnetism resulting from the hydrolysis and polymerization of aqueous Fe(III) has interested research workers for more than 60 years.[3,4] Despite the importance of basic polynuclear Fe(III) aquo species to the inorganic, geochemical, and bioinorganic chemistry of iron, their structural, magnetic, and electronic properties are still neither adequately characterized nor clearly understood. The magnetic properties of even the simplest polymerization product, the so-called aquo dimer of probable structure $[(H_2O)_4Fe(OH)_2Fe(H_2O)_4]^{4+}$, remain subject to dispute.

The unavailability of crystalline salts of the aquo dimer has prevented its definitive study by the usual combination of x-ray crystallographic and magnetochemical techniques. A number of workers have attempted to determine the magnetic properties of this dimer as either a solution species or as an adsorbed species on a sulfonate-type ion exchange resin.[3-7] Both techniques are plagued by the presence of substantial amounts of $S = 5/2$ Fe(III) monomers and the possible irreversible formation of high molecular weight Fe(III) polymers. (It would appear, however, that at 25°C the magnetic properties of the polymers and aquo dimer may not be grossly dissimilar.[5]) While all workers have agreed that the dimer exhibits antiferromagnetic spin–spin coupling, estimates of the magnetic moment (μ) per Fe(III) at 25°C have ranged from 0 to ≈ 3.7 μ_B. In terms of a model based on the usual $-2J\bar{S}_1 \cdot \bar{S}_2$ exchange Hamiltonian, the upper figure of ≈ 3.7 μ_B corresponds to $J \simeq -40$ cm^{-1}. It is not yet certain whether the -40 cm^{-1} value is in error or is related to the marked variation in J values observed for a series of $[Cu_2(OH)_2]^{2+}$ complexes having different Cu-OH-Cu bridging angles.[8] Substantially smaller spin–spin coupling (10–17 cm^{-1}) has recently been observed for crystalline Fe(III) chelates containing $[Fe_2(OH)_2]^{4+}$ or $[Fe_2(alkoxo)_2]^{4+}$ bridging units;[9-11] however, structural information derived from x-ray diffraction data is available only for two $[Fe_2(alkoxo)_2]^{4+}$ type dimers.[11] We have chosen to characterize the $[Fe_2(OH)_2]^{4+}$ unit in detail in order to determine its magnetic properties and variation, if any, with the geometric and chemical features of the bridging and nonbridging ligands. We report here the crystal structures and magnetic properties of $[Dipic(H_2O)FeOH]_2$ (Dipic = 2,6-pyridinedicarboxylate) and $[Chel(H_2O)FeOH]_2 \cdot 4H_2O$ (Chel = 4-hydroxo-2,6-pyridinedicarboxylate).

Experimental Section

(1) Preparation and Characterization of Complexes. The ligand 2,6-pyridinedicarboxylic acid (Aldrich Chemical Co.) was used as received. $[Dipic(H_2O)FeOH]_2$ was obtained as green prisms by maintaining equimolar mixtures of 2,6-pyridinedicarboxylic acid, $FeCl_3 \cdot 6H_2O$, and urea at 90°C for 24 hr. In a typical experiment, a 1-l. aqueous solution 0.05 M in each reactant yielded 7.5 g (60%) of product which was collected by filtration, washed with H_2O (low solubility at 25°C), and air-dried. All solutions of reactants used to prepare the complexes were prefiltered through 0.22 μm pore size millipore filters. A solution of the product in cold aqueous $HClO_4$ gave a negative test for Cl^-. Anal. Calcd for $FeC_7NH_6O_3$: Fe, 21.82; C, 32.84; N, 5.47; H, 2.36. Found: Fe, 20.8 (iodometry); C, 32.71; N, 5.48; H, 2.01.

Chelidamic acid (Aldrich Chemical Co.) was received as an orange-brown powder and was purified by a variation of a published procedure.[12] Sufficient concentrated NH_3 was added to dissolve a slurry of 50 g of the crude material in 350 ml of hot H_2O (final pH ≈ 3.5). After the dark brown solution was stirred with 15 g of activated charcoal for 15 min and filtered, the product was precipitat-

Table I. Crystal Data

	$[Dipic(H_2O)FeOH]_2$		$[Chel(H_2O)FeOH]_2 \cdot 4H_2O$
	Body-centered	Primitive	Primitive
Space group	I_1	P_1	P_1
Z	2	1	1
a (Å)	11.085 (7)	8.844 (4)	7.972 (4)
b (Å)	11.001 (5)	11.001 (5)	11.106 (4)
c (Å)	7.303 (4)	7.303 (4)	7.051 (3)
α (deg)	94.09 (4)	94.06 (4)	67.71 (3)
β (deg)	89.87 (10)	111.56 (10)	112.73 (3)
γ (deg)	96.46 (4)	131.54 (4)	95.81 (4)
d_{obsd} (g/cm^3)	—	1.93 (1)	1.92 (1)
d_{calcd} (g/cm^3)	—	1.927	1.923
V (Å^3)	882.6	441.3	532.0
μ (cm^{-1})	—	17.7	15.0
λ (Å)	—	0.71069	0.71069

Transformation matrix: $\begin{pmatrix} 1/2 & -1/2 & -1/2 \\ 0 & 1 & 0 \\ 0 & 0 & 1 \end{pmatrix} \begin{pmatrix} h_I \\ k_I \\ l_I \end{pmatrix} = \begin{pmatrix} h_P \\ k_P \\ l_P \end{pmatrix}$

ed by lowering the pH to approximately 2.5 with concentrated HCl. A repetition of this procedure afforded a light yellow crystalline product which decomposed with gas evolution at 260°C (uncorrected, lit. 248–250°C).[12]

The preparation of $[Chel(H_2O)FeOH]_2 \cdot 4H_2O$ was similar to that of $[Dipic(H_2O)FeOH]_2$; a 1-l. aqueous solution that contained 0.05 M each of $FeCl_3 \cdot 6H_2O$, urea, and chelidamic acid yielded 10.1 g (65%) of a green crystalline product which also gave a negative test for Cl^-. Anal. Calcd for $FeC_7NH_{16}O_9$: Fe, 18.13; C, 27.30; N, 4.65; H, 3.27. Found: Fe, 18.0 (iodometry); C, 27.72; N, 4.65; H, 3.61.

Identical procedures, except for longer reaction periods (several days), were used to prepare the Cr(III) and Al(III) analogues of $[Chel(H_2O)FeOH]_2 \cdot 4H_2O$. On the basis of similar crystal morphologies and x-ray powder diffraction patterns, these three complexes appear to be isostructural. However, these observations are insufficient to ascertain whether the Cr(III) and Al(III) analogues crystallize in space group $P\bar{1}$ (as does the Fe(III) complex) or in space group $P1$.

The urea hydrolysis procedure was also used to prepare crystalline $[Dipic(H_2O)Cr(OH)]_2$ and $[Dipic(H_2O)Al(OH)]_2$. These complexes were isostructural (powder diffraction and crystal morphology), but different from the Fe(III) analogue. However, a crystallographic study of $[Dipic(H_2O)Cr(OH)]_2$ showed that its *molecular structure* is comparable to that reported below for $[Dipic(H_2O)Fe(OH)]_2$.[13]

(2) Spectroscopic and Magnetic Measurements. Variable temperature magnetic susceptibility studies were performed in the laboratory of Professor H. B. Gray with a PAR FM-1 vibrating sample magnetometer equipped with an Andonian Dewar; the apparatus and techniques used to collect the data have been described elsewhere.[14] Diamagnetic corrections of 114×10^{-6} and 152×10^{-6} cgs per Fe(III) were used for $[Dipic(H_2O)FeOH]_2$ and $[Chel(H_2O)FeOH]_2 \cdot 4H_2O$, respectively; these were calculated from Pascal's constants.[15] Infrared spectra were measured with a Perkin-Elmer Model 225 spectrometer. Reactions run at 1/50th scale in D_2O were used to prepare the deuterated complexes.

Microscopic examination of both Fe(III) complexes indicated that they were obtained as pure single phases. X-Ray powder diffraction patterns of the bulk phases (used for the magnetic and spectral measurements) corresponded to the patterns calculated from the single-crystal data.

(3) X-Ray Data and Structure Solution: $[Dipic(H_2O)FeOH]_2$. A crystal approximately $0.28 \times 0.10 \times 0.10$ mm was mounted along its a axis in a sealed capillary. Preliminary Weissenberg and precession photographs revealed a body-centered triclinic cell (I_1 or $I\bar{1}$) with the systematic absence $h + k + l = 2n + 1$. Subsequent axis transformation and solution of the structure revealed $P\bar{1}$ as the correct space group.

Unit cell parameters were obtained by a least-squares fit of 33 moderately intense reflections using graphite monochromated Mo Kα radiation (λ 0.71069 Å) and an Enraf-Nonius CAD-3 automated diffractometer. Values of the centered and primitive cell parameters are given in Table I along with the transformation matrix relating body-centered and primitive reflection indices. The density of 1.927 g/cm^3 calculated for $Z = 1$ (primitive cell) agreed well with the value of 1.93 (1) g/cm^3 measured by floatation of several crystals in a solution of CBr_4 in CCl_4.

Diffractometer data based on the centered cell were collected at 22 ± 1°C. Graphite-monochromated Mo Kα radiation was detected with a scintillation counter and a pulse height analyzer set to admit approximately 90% of the Kα peak. A θ–2θ scan was used to collect a unique data set to a maximum of $2\theta = 60°$. Reflections with $2\theta < 4°$ were shielded by the beam stop and were not recorded. The scan range S was a function of θ chosen according to $S = (1.50 + 0.1 \tan \theta)°$. Each reflection was scanned before being recorded, and zirconium foil attenuators were automatically inserted if the intensity of the diffracted beam exceeded 6000 counts/sec. A circular aperture 0.5 mm in diameter was placed 4.1 cm from the crystal. Background measurements were made at the beginning and end of each scan with the counter stationary; the total time for background counts equalled the scan time. The scan rate was 1/6° per second, and each reflection was scanned repeatedly to a maximum of six scans or until 6000 total counts were obtained. Intensities were placed on a common scale by dividing by the number of scans. The intensity of a standard reflection, measured at 50 reflection intervals, was consistent to ±2% and showed no significant trend.

A total of 2603 independent reflections was collected; these were reduced using the transformation matrix and then corrected for Lorentz and polarization effects. The linear absorption coefficient, $\mu = 17.7$ cm^{-1} for Mo Kα radiation, is so small that absorption corrections were not considered necessary for a crystal of the size used to collect data. Standard deviations were assigned to F^2 values according to

$$\sigma(F^2) = \frac{1}{LP}(N_t + (0.02N_n)^2)^{1/2}$$

where N_t is the total count (scan plus background), N_n is the net count, and 0.02 is an estimate of instrumental instability. The overall scale factor was initially estimated using Wilson's method and was then refined.

The structure was solved by the heavy atom method using 1436 reflections with $F^2 \geq 3\sigma(F^2)$ and refined using full-matrix least-squares techniques.[16] We initially assumed that the dimer was centrosymmetric. The space group $P\bar{1}$ has two general positions, and the presence of one dimer per unit cell requires one monomer per asymmetric unit. Approximate coordinates for the iron atom and two oxygen atoms were obtained from a normal sharpened Patterson map. A difference map based on the iron and oxygen phases revealed the coordinates of the remaining non-hydrogen atoms. With all non-hydrogen scattering matter present, the initial agreement factor $R_F = \Sigma||F_o| - |F_d||/\Sigma|F_o|$ was 0.211.

Isotropic refinement was initiated using atomic scattering factors from Cromer and Waber for Fe, O, N, C, and H.[17] All atoms were treated as neutral species. Both real and imaginary parts of the anomalous dispersion corrections were applied to Fe.[18] Initial refinement was based on F^2, and weights were set according to $w = 1/\sigma^2$. Three refinement cycles of all atomic positional and thermal parameters reduced R_F to 0.104. Two additional cycles of refinement with anisotropic thermal parameters for all non-hydrogenic atoms reduced R_F to 0.076.

Further refinement was based on F. A weighting scheme, chosen by an analysis of variance,[19] led to the following assignments for $\sigma(F_o)$:

$$\sigma(F_o) = 1.03 - 0.014|F_o|; 2.90 < |F_o| \leq 15.3$$

$$\sigma(F_o) = 0.054|F_o| - 0.012; |F_o| > 15.3$$

Two cycles of refinement reduced R_F to 0.064 and $R_{wF} = [\Sigma w(F_o - F_c)^2/\Sigma wF_o^2]^{1/2}$ to 0.078. The pyridine ring hydrogen positions were calculated, and hydrogen atoms were included at these positions for further refinement with isotropic temperature factors equal to the overall temperature factor obtained from the Wilson plot. Hydrogen atom positional and thermal parameters were not refined. Two additional cycles of refinement reduced R_F to 0.059 and R_{wF} to 0.075. A difference Fourier map at this point revealed

Table II. Fractional Atomic Coordinates[a] and Thermal Parameters[b] for $[Dipic(H_2O)FeOH]_2$ and $[Chel(H_2O)FeOH]_2 \cdot 4H_2O$

Atom	x	y	z	β_{11} or B	β_{22}	β_{33}	β_{12}	β_{13}	β_{23}
				$[Dipic(H_2O)FeOH]_2$					
Fe	−2373.8 (10)	1347.9 (7)	589.5 (11)	121.3 (8)	48.5 (6)	79.6 (12)	53.8 (5)	30.7 (8)	3.4 (6)
O(1)	−1188 (5)	3805 (3)	1326 (6)	205 (5)	79 (3)	112 (7)	105 (3)	50 (5)	18 (4)
O(2)	1621 (5)	6693 (4)	3858 (6)	235 (5)	71 (3)	128 (7)	101 (3)	75 (5)	22 (4)
O(3)	−1647 (5)	−64 (4)	1145 (6)	215 (6)	67 (3)	128 (8)	91 (3)	64 (5)	12 (4)
O(4)	951 (5)	12 (4)	3453 (6)	283 (5)	121 (4)	165 (8)	161 (3)	105 (5)	49 (4)
O(5)	−5713 (5)	−559 (4)	−1933 (5)	173 (5)	98 (4)	74 (7)	89 (3)	52 (5)	6 (4)
O(6)	−903 (5)	2007 (4)	−1210 (6)	211 (5)	96 (4)	137 (8)	113 (3)	78 (5)	41 (4)
N	877 (5)	3133 (4)	3649 (6)	157 (6)	67 (4)	73 (7)	79 (3)	54 (5)	15 (4)
C(1)	1999 (6)	4825 (5)	4647 (7)	141 (7)	60 (5)	115 (10)	65 (4)	79 (6)	27 (5)
C(2)	4096 (7)	6015 (6)	6765 (8)	165 (8)	89 (5)	99 (10)	79 (5)	57 (7)	14 (5)
C(3)	4997 (8)	5420 (6)	7779 (8)	180 (8)	116 (6)	124 (11)	96 (5)	58 (8)	38 (6)
C(4)	3811 (7)	3646 (6)	6660 (8)	170 (8)	104 (6)	114 (10)	94 (5)	71 (7)	37 (6)
C(5)	1753 (6)	2563 (5)	4557 (7)	159 (7)	82 (5)	95 (9)	90 (4)	67 (6)	32 (5)
C(6)	714 (6)	5144 (5)	3180 (7)	168 (7)	62 (4)	108 (10)	83 (4)	74 (6)	25 (5)
C(7)	254 (7)	671 (5)	2967 (8)	184 (7)	74 (5)	130 (11)	91 (4)	89 (7)	32 (5)
H(C(2))	5004	7379	7622	1.69					
H(C(3))	6640	6317	9447	1.69					
H(C(4))	4500	3177	7497	1.69					
H(O(5))	−3600	1000	3600	1.69					
H(O(6)-1)	−1000	1200	−2000	1.69					
H(O(6)-2)	−800	2600	−1800	1.69					
				$[Chel(H_2O)FeOH]_2 \cdot 4H_2O$					
Fe	−1363.2 (9)	1038.5 (7)	−2042.2 (12)	55.2 (9)	26.2 (5)	129 (2)	−1.8 (6)	45 (1)	−28 (1)
O(1)	−3810 (4)	145 (3)	−2489 (5)	90 (5)	38 (3)	190 (10)	−13 (3)	70 (6)	−44 (3)
O(2)	−6702 (4)	279 (3)	−2867 (5)	92 (5)	51 (3)	216 (10)	−36 (3)	91 (6)	−65 (4)
O(3)	86 (4)	2647 (3)	−2128 (5)	60 (5)	43 (3)	213 (10)	−9 (3)	69 (6)	−48 (3)
O(4)	208 (4)	4679 (3)	−2237 (6)	88 (5)	41 (3)	283 (12)	−21 (3)	93 (7)	−59 (4)
O(5)	586 (4)	−191 (3)	−1229 (5)	96 (5)	52 (3)	132 (9)	18 (3)	57 (6)	−37 (3)
O(6)	−2007 (5)	1545 (3)	−5358 (5)	113 (6)	47 (3)	148 (10)	−18 (3)	67 (6)	−41 (3)
O(7)	−6394 (4)	4979 (3)	−2346 (6)	84 (5)	49 (3)	261 (12)	1 (3)	92 (6)	−56 (4)
O(8)	3766 (5)	2478 (4)	2479 (6)	146 (7)	70 (4)	276 (14)	9 (4)	92 (8)	−63 (4)
O(9)	308 (5)	2769 (4)	2871 (6)	159 (6)	48 (3)	307 (14)	−14 (4)	141 (8)	−50 (4)
N	−3121 (5)	2378 (4)	−2299 (6)	67 (6)	35 (3)	113 (11)	−12 (4)	48 (6)	−31 (4)
C(1)	−4801 (6)	2055 (4)	−2414 (7)	60 (6)	35 (4)	96 (12)	−7 (4)	41 (7)	−22 (4)
C(2)	−5994 (6)	2868 (5)	−2412 (7)	62 (7)	40 (4)	125 (13)	−9 (4)	49 (8)	−26 (5)
C(3)	−5371 (6)	4084 (5)	−2297 (7)	58 (6)	42 (4)	121 (13)	−4 (4)	49 (8)	−28 (4)
C(4)	−3577 (6)	4414 (4)	−2174 (8)	76 (7)	30 (4)	143 (14)	−5 (4)	51 (8)	−22 (5)
C(5)	−2507 (6)	3523 (4)	−2200 (7)	58 (7)	31 (4)	100 (12)	−8 (4)	36 (7)	−21 (4)
C(6)	−5184 (6)	721 (4)	−2600 (7)	69 (7)	31 (4)	104 (13)	−8 (4)	38 (8)	−17 (4)
C(7)	−578 (6)	3654 (5)	−2166 (7)	68 (6)	45 (4)	140 (14)	−8 (4)	69 (8)	−28 (5)
H(C(2))	−7345	2568	−2490	76	33	125	−5	62	−36
H(C(4))	−3044	5318	−1980	71	33	128	1	57	−36
H(C(5))	1110	−365	−2315	106	52	146	11	58	−30
H(O(6)-1)	−1200	1900	−6000	109	45	142	−9	57	−38
H(O(6)-2)	−2800	1000	−6000	109	45	142	−9	57	−38
H(O(7))	−7400	4900	−2200	95	48	243	3	95	−52
H(O(8)-1)	3800	1900	1800	148	68	267	5	92	−59
H(O(8)-2)	4800	2400	2600	148	68	267	5	92	−59
H(O(9)-1)	600	3500	3400	155	51	297	−13	134	−50
H(O(9)-2)	1400	2700	2600	155	51	297	−13	134	−50

[a] Atomic coordinates are $\times 10^4$. [b] Anistropic thermal parameters are $\times 10^4$; the form of the anisotropic thermal ellipsoid is $\exp[-(\beta_{11}h^2 + \beta_{22}k^2 + \beta_{33}l^2 + 2\beta_{12}hk + 2\beta_{13}hl + 2\beta_{23}kl)]$.

the coordinates of the three remaining hydrogen atoms. Two additional cycles of refinement resulted in final values of $R_F = 0.052$ and $R_{wF} = 0.067$. For the last refinement cycle, all positional and thermal parameter changes were within their estimated standard deviation. A final difference map showed a general background of 0.5 e/Å^3 and no peaks larger than 0.9 e/Å^3; all peaks above background were residuals of known atoms.[20]

(4) X-Ray and Structure Solution: $[Chel(H_2O)FeOH]_2 \cdot 4H_2O$. Data collection and reduction were equivalent to that for $[Dipic(H_2O)FeOH]_2$ with the following exceptions: (1) the crystal size was approximately 0.25 × 0.25 × 0.20 mm; (2) the scan range S was selected as $S = (1.20 + 0.87 \tan \theta)°$ based on analysis of representative peak profiles; and (3) cell constants were determined from a least-squares refinement of 16 moderately intense reflections centered on the diffractometer. The calculated density of 1.923 g/cm^3 agreed well with the value of 1.92 (1) g/cm^3 measured by flotation of several crystals in a solution of CCl_4 and $CHBr_2CHBr_2$. Pertinent crystal data for $[Chel(H_2O)FeOH]_2 \cdot 4H_2O$ are shown in Table I.

The structure was solved by the heavy atom method using 1543 reflections with $F^2 \geq 3\sigma(F^2)$ from a total of 3329 measured independent diffraction maxima. With all non-hydrogen scattering matter present, R_F was 0.18. Anisotropic refinement using weights derived from counting statistics reduced R_F to 0.064. An analysis of variance then led to the following assignments for $\sigma(F_o)$:

$$\sigma(F_o) = 1.22 - 0.030|F_o|; 2.0 \leq |F_o| \leq 20.0$$

$$\sigma(F_o) = 0.008|F_o| + 0.456; |F_o| > 20.0$$

Hydrogen atoms were located as above. These were added as fixed atom contributors to the structure factor and assigned anisotropic temperature factors equal to those of the carbon atoms to which they are bonded. Five cycles of anisotropic refinement (excluding H) reduced R_F and R_{wF} to their final values of 0.044 and 0.049, respectively. All positional and thermal parameter changes were within their estimated standard deviation for the final refinement cycle. A final difference map showed a general background of 0.4 e/Å^3 and no peaks larger than 0.6 e/Å^3; all peaks above background were residuals of known atoms.

Final atomic parameters for both structures, together with estimated standard deviations from the least-squares refinement, are given in Table II. A view of both dimers, showing the atom num-

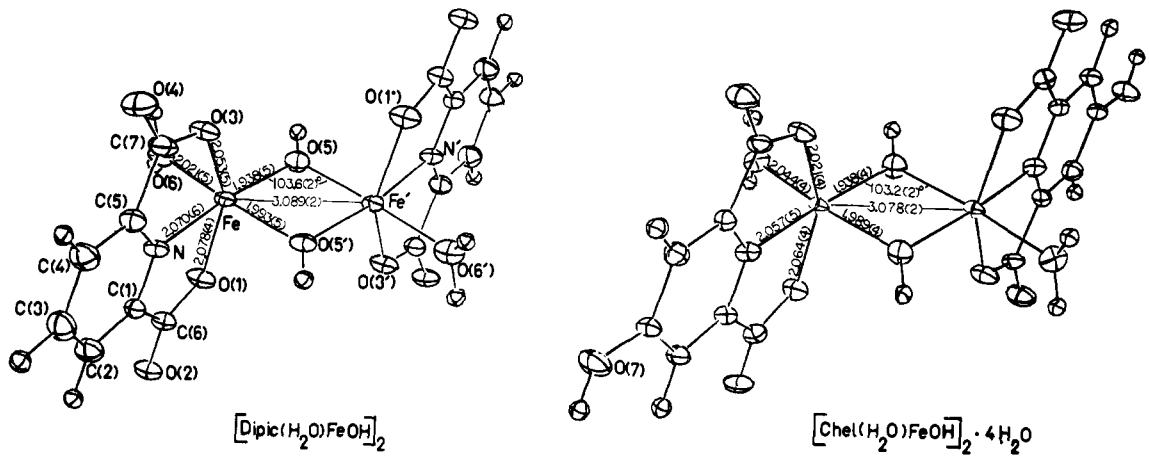

Figure 1. Molecular structure of $[Dipic(H_2O)FeOH]_2$ showing the atom numbering scheme and molecular structure of $[Chel(H_2O)FeOH]_2{\cdot}4H_2O$. The numbering scheme is similar to that for $[Dipic(H_2O)FeOH]_2$; the ring hydroxyl atom is O(7). Lattice oxygen atoms have been omitted for clarity.

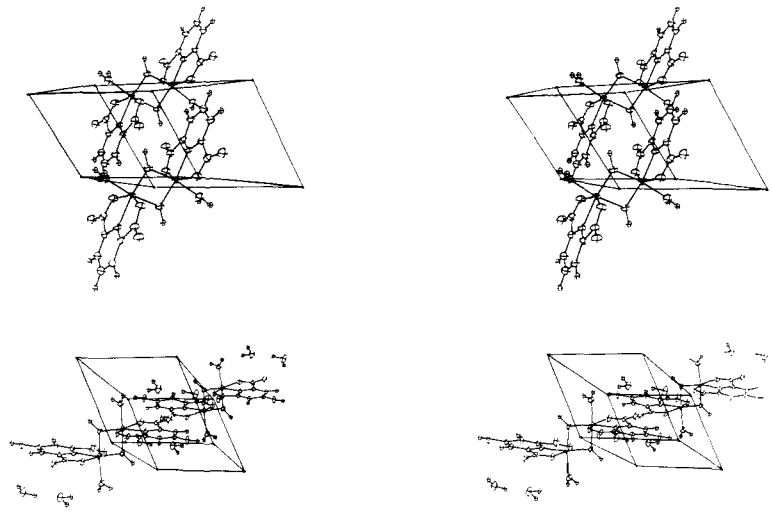

Figure 2. (Top) Stereoscopic packing diagram for $[Dipic(H_2O)FeOH]_2$. The origin of the unit cell has been translated ½ along *a* in order to clarify both the centrosymmetric nature of this dimeric complex and its similarity to the one shown below. (Bottom) Stereoscopic packing diagram for $[Chel(H_2O)FeOH]_2{\cdot}4H_2O$.

bering scheme, is given in Figure 1. Lists of observed and calculated structure factors are available.[20]

Description of the Structures

Both structures consist of centrosymmetric $[L(H_2O)FeOH]_2$ dimeric units in which crystallographically equivalent Fe(III) ions are bridged by two hydroxyl groups. The Fe(III) ions have a distorted octahedral coordination geometry. Chel and Dipic occupy three coordination sites; the remaining three are occupied by the two bridging hydroxyl groups and a terminal water molecule. Although the pyridine rings are situated on opposite sides of the distorted edge-shared octahedral units in both complexes, there appears to be no compelling intramolecular steric grounds for exclusive formation of the "trans" isomer. As a referee as noted, this result may be caused by crystal packing forces. A comparison of bond distances and angles for both structures (Table III) shows that they are strikingly similar.

The largest distortion from octahedral symmetry is evidenced by the angles O(1)-Fe-O(3) (149.7 (150.6)°) and is due to the limited bite of the tridentate ligand. This distortion is also demonstrated by deviations from the least-squares planes given in Table IV. Atoms N, O(6), O(6'), and O(5') (plane 1), which do not involve the carboxylate oxygen atoms, show a maximum deviation from planarity of 0.11 Å. The Fe(III) ions lie on plane 1 within experimental error. In contrast, atoms O(1), O(3), O(5'), and O(6) (plane 3) show much larger deviations from planarity. The Fe(III) ions are displaced more than 0.15 Å from these planes.

The Fe···Fe separations in $[Chel(H_2O)FeOH]_2{\cdot}4H_2O$ and $[Dipic(H_2O)FeOH]_2$ of 3.078 and 3.089 Å, respectively, are comparable, although they are nonequivalent (3.8σ) within experimental error. Both separations are large enough to effectively preclude significant direct overlap of metal ion orbitals based on the ionic radius (0.65-0.79 Å) of high-spin six-coordinate Fe(III).[21] The Fe-OH-Fe bridging angles (103.6 (103.2)°) in the strictly planar $[Fe_2(OH)_2]^{4+}$ units are equivalent in both structures, as are the corresponding Fe-OH distances. Thus, the only significant difference between the $[Fe_2(OH)_2]^{4+}$ units in both structures is the Fe···Fe distance, and this difference is small.

Bond distances and angles of the Dipic and Chel ligands are similar and agree with those reported by other workers for free and complexed Dipic.[22] For this reason, they will not be considered in detail here. We have been unable to locate prior crystallographic studies of either free or complexed Chel. Since the ring hydroxyl hydrogen atom was located on a difference map, and the C(4)-O(7) bond length

Table III. Bond Distances (Å) and Angles (deg) in $[Dipic(H_2O)FeOH]_2$ and $[Chel(H_2O)FeOH]_2 \cdot 4H_2O$[a]

Atoms	Distance		Atoms	Distance	
Fe...Fe'	3.089 (2)	(3.078 (2))	Fe–O(5')	1.993 (5)	(1.989 (4))
Fe–O(1)	2.078 (4)	(2.064 (4))	Fe–O(6)	2.021 (5)	(2.044 (4))
Fe–O(3)	2.053 (5)	(2.021 (4))	Fe–N	2.070 (6)	(2.057 (5))
Fe–O(5)	1.938 (5)	(1.938 (4))			
O(1)–C(6)	1.261 (5)	(1.285 (7))	C(1)–C(2)	1.389 (6)	(1.377 (8))
O(2)–C(6)	1.252 (6)	(1.231 (6))	C(1)–C(6)	1.501 (8)	(1.527 (7))
O(3)–C(7)	1.285 (6)	(1.272 (7))	C(2)–C(3)	1.393 (10)	(1.412 (7))
O(4)–C(7)	1.225 (8)	(1.235 (6))	C(3)–C(4)	1.416 (9)	(1.417 (7))
O(7)–C(3)	—	(1.330 (7))	C(4)–C(5)	1.379 (6)	(1.380 (8))
N–C(1)	1.344 (7)	(1.330 (6))	C(5)–C(7)	1.517 (7)	(1.522 (7))
N–C(5)	1.326 (8)	(1.333 (6))			
O(5)–H(O(5))	1.033	(1.083)	C(2)–H(C(2))	1.091	(1.083)
O(6)–H(O(6)-1)	0.956	(0.902)	C(3)–H(C(3))	1.094	
O(6)–H(O(6)-2)	0.782	(0.938)	C(4)–H(C(4))	1.091	(1.086)
O(7)–H(O(7))		(0.839)			
O(8)–H(O(8)-1)		(0.943)			
O(8)–H(O(8)-2)		(0.805)			
O(9)–H(O(9)-1)		(0.988)			
O(9)–H(O(9)-2)		(0.976)			

Hydrogen Bonding Contact Distances

$[Chel(H_2O)FeOH]_2 \cdot 4H_2O$		$[Dipic(H_2O)FeOH]_2$	
O(1)···O(8)	2.914 (6)	O(6)···O(4)	2.630 (7)
O(2)···O(5)	2.743 (6)	O(6)···O(2)	2.721 (7)
O(2)···O(6)	2.691 (6)		
O(4)···O(7)	2.723 (6)		
O(4)···O(9)	2.745 (6)		
O(6)···O(9)	2.610 (6)		
O(8)···O(9)	2.935 (7)		

Atoms	Angle		Atoms	Angle	
Fe'–Fe–O(1)	102.9 (2)	(103.4 (1))	O(1)–C(6)–O(2)	125.9 (5)	(124.9 (5))
Fe'–Fe–O(3)	102.3 (2)	(100.5 (1))	O(3)–C(7)–O(4)	126.0 (4)	(124.8 (5))
Fe'–Fe–O(6)	134.0 (1)	(131.8 (1))	O(1)–C(6)–C(1)	115.7 (5)	(114.1 (4))
Fe–O(1)–C(6)	118.9 (4)	(119.4 (3))	O(2)–C(6)–C(1)	118.4 (3)	(121.1 (5))
Fe–O(3)–C(7)	119.7 (4)	(120.6 (3))	O(3)–C(7)–C(5)	114.2 (5)	(114.0 (4))
Fe–O(5)–Fe'	103.6 (2)	(103.2 (2))	O(4)–C(7)–C(5)	119.8 (4)	(121.2 (5))
Fe–N–C(1)	118.2 (4)	(119.6 (2))	O(7)–C(3)–C(2)	—	(123.6 (4))
Fe–N–C(3)	176.6 (3)	(175.7 (2))	O(7)–C(3)–C(4)	—	(116.6 (4))
Fe–N–C(5)	119.1 (4)	(118.9 (4))	N–C(1)–C(2)	119.6 (3)	(122.4 (5))
O(1)–Fe–O(3)	149.7 (1)	(150.6 (2))	N–C(1)–C(6)	111.4 (3)	(110.9 (4))
O(1)–Fe–O(5)	108.5 (2)	(110.5 (2))	N–C(5)–C(4)	121.6 (5)	(121.4 (4))
O(1)–Fe–O(5')	92.1 (1)	(90.9 (1))	N–C(5)–C(7)	111.1 (3)	(110.3 (5))
O(1)–Fe–O(6)	86.5 (2)	(86.9 (2))	C(3)–O(7)–H(O(7))	—	(128.8 (4))
O(3)–Fe–O(5)	101.7 (2)	(98.8 (2))	C(1)–N–C(5)	122.7 (3)	(121.4 (5))
O(3)–Fe–O(5')	97.9 (2)	(97.7 (1))	C(1)–C(2)–C(3)	118.5 (5)	(117.2 (4))
O(3)–Fe–O(6)	87.8 (2)	(89.8 (1))	C(1)–C(2)–H(C(2))	120.8 (6)	(120.3 (5))
O(5)–Fe–O(5')	76.4 (2)	(76.8 (2))	C(2)–C(1)–C(6)	129.0 (5)	(126.7 (4))
O(5)–Fe–O(6)	95.3 (2)	(93.1 (2))	H(C(2))–C(2)–C(3)	120.7 (4)	(122.4 (5))
O(5')–Fe–O(6)	170.7 (1)	(168.2 (2))	C(2)–C(3)–C(4)	120.6 (4)	(119.8 (5))
O(1)–Fe–N	75.5 (2)	(75.7 (2))	C(2)–C(3)–H(C(3))	120.6 (5)	—
O(3)–Fe–N	75.5 (2)	(75.8 (2))	H(C(3))–C(3)–C(4)	118.8 (7)	—
O(5)–Fe–N	168.0 (2)	(168.3 (2))	C(3)–C(4)–C(5)	116.9 (6)	(117.8 (5))
O(5')–Fe–N	92.3 (2)	(93.5 (2))	C(3)–C(4)–H(C(4))	119.8 (4)	(120.8 (5))
O(6)–Fe–N	96.3 (2)	(97.1 (2))	H(C(4))–C(4)–C(5)	123.2 (5)	(121.3 (5))
			C(4)–C(5)–C(7)	127.2 (6)	(128.3 (4))

[a] Values for $[Chel(H_2O)FeOH]_2 \cdot 4H_2O$ are given in parentheses.

is typical of that for a carbon–oxygen single bond,[23] Chel is clearly bonded in the enol[12] form. The pyridine ring atoms are coplanar within experimental error (plane 4). However, rather large deviations from planarity are found for the entire ligand in both structures (plane 5); these are attributed primarily to the nonbonding carboxylate oxygen atoms O(2) and O(4), both of which are approximately 0.15 Å removed from the plane of the remaining ligand atoms. The iron atoms and the bridging hydroxyl oxygen atoms show large deviations from this plane in the opposite direction; this gives a further indication of the distorted geometry in both complexes.

In the Dipic structure, individual dimeric units are linked by a hydrogen bonding network involving the coordinated water hydrogen atoms and the carboxylate oxygen atoms of neighboring molecules. In the Chel structure, an extensive hydrogen bonding network, involving the lattice and coordinated water molecules, the Chel hydroxyl group, and the carboxylate oxygen atoms O(2) and O(4), links dimers together. Intermolecular hydrogen bonding distances are listed in Table III, while Figure 2 illustrates the packing for both structures. No evidence was found in either structure for intramolecular hydrogen bonding. Although Dipic and Chel dimers show different intermolecular bonding, this does not appear to affect the structural parameters of the $[Fe_2(OH)_2]^{4+}$ units significantly; however, hydrogen bonding may in part account for the rather large deviations of atoms O(2) and O(4) from the planes of the dicarboxylate

Table IV. Deviations from Least-Squares Planes (Å)[a,b]

(1) Plane defined by N, O(6), O(5), O(5')

	Distance from Plane				
N	0.058	(0.111)	O(5')	0.073	(−0.103)
O(6)	−0.058	(−0.099)	Fe	0.002	(−0.003)
O(5)	−0.073	(0.092)			

(2) Plane defined by O(1), O(3), N, O(5)

	Distance from Plane				
O(1)	−0.147	(−0.116)	O(5)	0.116	(0.064)
O(3)	−0.155	(−0.126)	Fe	−0.051	(−0.056)
N	0.186	(0.177)			

(3) Plane defined by O(1), O(3), O(6), O(5')

	Distance from Plane				
O(1)	0.344	(−0.358)	O(5')	−0.313	(0.303)
O(3)	0.327	(−0.336)	Fe	−0.185	(0.158)
O(6)	−0.357	(0.390)			

(4) Plane defined by N, C(1), C(2), C(3), C(4), C(5)

	Distance from Plane				
C(1)	−0.010	(−0.002)	C(4)	0.001	(0.004)
C(2)	−0.004	(0.000)	C(5)	−0.015	(−0.006)
C(3)	0.008	(0.0002)	N	0.020	(0.003)

(5) Plane defined by N, C(1)–C(7), O(1)–O(4)

	Distance from Plane				
N	0.089	(0.037)	O(1)	0.023	(0.041)
C(1)	0.036	(0.030)	O(2)	−0.135	(−0.110)
C(2)	0.022	(0.024)	O(3)	0.074	(0.035)
C(3)	0.041	(0.027)	O(4)	−0.181	(−0.123)
C(4)	0.059	(0.035)	O(7)	—	(−0.012)
C(5)	0.061	(0.028)	Fe	0.247	(0.199)
C(6)	−0.021	(−0.012)	O(5)	0.779	(0.685)
C(7)	−0.010	(−0.013)			

[a] Values for $[Chel(H_2O)FeOH]_2 \cdot 4H_2O$ are given in parentheses. [b] Unit weights were employed in the calculation of all planes.

ligands. To a good approximation, both structures may be regarded as consisting of virtually discrete and magnetically dilute dimers.

Infrared Spectra. Selected OH(D) modes of the title complexes and of related dimers having $Cr_2(OH)_2^{4+}$ and $Al_2(OH)_2^{4+}$ units are presented in Table V. Powder diffraction studies indicate that $[Chel(H_2O)FeOH]_2 \cdot 4H_2O$ is isostructural with its Cr(III) and Al(III) analogues. Similarly, $[Dipic(H_2O)CrOH]_2$ and $[Dipic(H_2O)AlOH]_2$ are isostructural, but exhibit a powder pattern different from that of the Fe(III) analogue. Crystallographic studies of $[Dipic(H_2O)CrOH]_2$ show that its molecular structure, but not its crystal structure, is comparable to that found for the Fe(III) analogue.[13] Thus a combination of isotopic and metal ion substitutions may be used to identify the OH(D) modes in the above series of dihydroxo bridged dimers. Except for a few instances in which a mode of interest was obscured by other vibrations, deuteration resulted in an isotopic red shift of $\sim\sqrt{2}$.

$Fe(OH)SO_4$ and $Fe(OH)CrO_4$ are isostructural lattice polymers containing chains of hydroxo bridged Fe(III) ions, e.g., $(FeOHFeOHFeOH)_\infty$. The identification of the stretching and deformation modes of the bridging OH at ~3500 and ~950 cm^{-1}, respectively, was facilitated by the absence of ligand/lattice water.[24] Comparable absorptions are exhibited by the dihydroxo bridged dimers (Table V). The series of Dipic complexes exhibits a broad strong absorption at 3410–3560 cm^{-1} assigned to the stretching mode of the bridging OH; the corresponding deformation mode appears at 900–980 cm^{-1}. Except for varying degrees of band splitting, these absorptions are similar for the Chel complexes. The OH stretching modes for $[Chel(H_2O)FeOH]_2 \cdot 4H_2O$ and its Cr(III) analogue have weak shoulders at higher energy. However, only a single deformation mode of the bridging OH (900 and 950 cm^{-1}, respectively) was observed for these two complexes. The Al(III) analogue exhibits about equally intense OH stretching modes at 3540 and 3430 cm^{-1} along with two corresponding OH deformation modes at 1020 and 950 cm^{-1}. We note that the Al(III) analogue was obtained as a single phase whose powder diffraction pattern essentially was identical with that of $[Chel(H_2O)FeOH] \cdot 4H_2O$. Such a comparison will not differentiate between the possible space groups of P_1 or $P\bar{1}$ for the Al(III) complex. However, factor and site group considerations indicate that two OH stretching and two OH deformation modes are allowed in both space groups.

All of the complexes exhibit a broad band system centered at 3000–3100 cm^{-1} which is assigned to the deformation modes of ligand and, for the Chel complexes, lattice H_2O. The corresponding OH_2 deformation mode, expected to appear at ~1600 cm^{-1}, is obscured by strong carboxylate absorption in that spectral region. However, a weak absorption at 1205–1225 cm^{-1} exhibited by all of the deuterated dimers may reasonably be assigned to the isotopically shifted deformation mode of the lattice/ligand H_2O molecules. Unique to the Chel complexes are absorptions at 3610–3630 and 1220–1245 cm^{-1} which are assigned to the stretching and deformation modes, respectively, of the ring OH group. Thus, the ir spectra reflect the fact that the Chel ligand is present in the enol, rather than keto, form.

Magnetic Susceptibility. Magnetic susceptibility data in the temperature range 85–300 K, corrected for diamagnetism, are presented as μ_{eff} per Fe(III) in Table VI. The usual spin-spin interaction model based on the exchange Hamiltonian $H = -2J\bar{S}_1 \cdot \bar{S}_2$ with $S_1 = S_2 = 5/2$, $g = 2.00$, and TIP = 0 leads to the relationship:

$$\mu_{eff}^2 = 12.006 \frac{55 + 30z^{10} + 14z^{18} + 5z^{24} + z^{28}}{11 + 9z^{10} + 7z^{18} + 5z^{24} + 3z^{28} + z^{30}}$$

where $z = \exp[-J/kT]$.[15] A J value for each temperature (Table VI) was obtained graphically from the experimental μ_{eff}^2 vs. T data and plots of μ_{eff}^2 vs. kT/J calculated using the above relationship. Average J values for $[Dipic(H_2O)FeOH]_2$ and $[Chel(H_2O)FeOH]_2 \cdot 4H_2O$ are −11.4 (4) and −7.3 (5) cm^{-1}, respectively. A more detailed analysis of the susceptibility data by least-squares fitting techniques supports the assumptions of $g = 2.00$ and TIP = 0 and yields the same J values. Thus, while both complexes exhibit only modest coupling, the coupling constant for the Dipic complex is clearly larger in magnitude than that of the Chel complex. Magnetic moments per Fe(III) calculated using these average J values in the above equation are also shown in Table VI. These moments are typically within 0.1 μ_B of those determined experimentally. Although the agreement between observed and calculated moments may be improved by using an additional parameter j' corresponding to a higher order exchange term in the Hamiltonian $[j'(\bar{S}_1 \cdot \bar{S}_2)^2]$, the significance of such a treatment is not clear, and higher order terms were neglected here.[25,26]

Discussion

$[Dipic(H_2O)FeOH]_2$ and $[Chel(H_2O)FeOH]_2 \cdot 4H_2O$ are the first two complexes for which the $Fe_2(OH)_2^{4+}$ unit has been characterized by x-ray crystallography. A related complex formulated as $[(Pic)_2FeOH]_2$ where Pic = pyridine-2-carboxylate has been previously characterized both as a solution[27] and as a crystalline species.[9] In contrast to the Fe(III)–Pic system, detailed studies of the solution equilibria of the Fe(III)–Dipic system gave no indication of dimer formation at 25°C.[27] Although we have observed that $[Dipic(H_2O)FeOH]_2$ precipitates from aqueous solutions of Na_2Dipic and Fe(III) at 25°C, no further attempts

Table V. Selected OH(D) Ir Modes (cm^{-1}) of $M_2(OH)_2^{4+}$ Complexes with Dipic and Chel

Mode[a]	$[Dipic(H_2O)MOH]_2$			$[Chel(H_2O)MOH]_2 \cdot 4H_2O$		
	M = Fe(III)	M = Cr(III)	M = Al(III)	M = Fe(III)	M = Cr(III)	M = Al(III)
Ring OH stretch	—	—	—	3630 m, sp	3610 m, sp	3620 m, sp
Ring OD stretch	—	—	—	2680 m, sp	2680 m, sp	2690 m, sp
Ring OH def	—	—	—	1220 m	1230 m	1245 m
Ring OD def	—	—	—	980 m	990 m	1000 m
Bridge OH stretch	3410 s, b	3470 s, b	3560 s, b	3460 w, sh 3400 s	3520 w, sh 3430 s	3540 s, sp 3430 s
Bridge OD stretch	2530 s	2580 s	2640 s	2615 w, sp 2510 s	2620 w, sp 2550 s	2620 s, sp 2530 s, sp
Bridge OH def	~900 m[b]	~940 m, sh[b]	980 s	~900 m[b]	950 m[b]	1020 m ~950 m[b]
Bridge OD def	~680[b]	720 m, sh	—[c]	695 m	728 m	~770 m[b] ~690 m[b]
Ligand–lattice OH_2 stretch	~3000 vb	~3070 vb	~3100 vb	~3100 vb	~3060 vb	~3070 vb
Ligand–lattice OD_2 stretch	~2250 vb	~2350 vb	~2350 vb	~2200 vb	~2240 vb	~2200 vb
Ligand–lattice OD_2 def	~1215 w, sh	1225 w	1236 w	1208 w	1205 w	1210 w

[a] Abbreviations used are: strong (s), medium (m), weak (w), broad (b), sharp (sp), shoulder (sh), very (v). [b] Overlaps other modes. Approximate band positions were estimated from spectral changes caused by isotopic substitution. [c] Obscured by other strong absorptions in the 750–800 cm^{-1} region.

Table VI. Magnetic Susceptibility Results for $[Dipic(H_2O)FeOH]_2$ and $[Chel(H_2O)FeOH]_2 \cdot 4H_2O$

	$[Dipic(H_2O)FeOH]_2$			$[Chel(H_2O)FeOH]_2 \cdot 4H_2O$		
T(°K)	μ_{eff}[a]	$-J$[b]	μ_{calcd} for $-J = 11.4$ cm^{-1}[c]	μ_{eff}[a]	$-J$[b]	μ_{calcd} for $-J = 7.3$ cm^{-1}[b]
299.6	4.86	12.1	4.93	5.24	7.8	5.28
285.9	4.82	12.0	4.88	5.21	7.8	5.25
273.2	4.81	11.6	4.83	5.21	7.4	5.22
260.5	4.78	11.4	4.78	5.17	7.4	5.18
246.5	4.73	11.3	4.71	5.13	7.4	5.15
232.4	4.68	11.1	4.64	5.15	7.9	5.10
217.7	4.62	10.9	4.56	5.10	6.8	5.04
202.2	4.54	10.8	4.47	5.06	6.6	4.97
186.0	4.40	11.0	4.35	4.97	6.8	4.89
168.6	4.26	11.0	4.21	4.88	6.7	4.79
150.0	4.08	11.0	4.03	4.73	6.9	4.65
129.5	3.81	11.3	3.79	4.56	6.8	4.47
106.0	3.44	11.6	3.47	4.20	7.2	4.18
96.0	3.23	12.0	3.30	3.94	7.7	4.03
85.0	3.03	11.9	3.10	3.71	7.9	3.84

[a] Calculated in μ_B at each temperature from the corrected molar susceptibility per Fe(III) using the formula $\mu_{eff}^2 = 7.998\ \chi^{corr}(T)$. [b] Calculated in cm^{-1} at each temperature by the procedure described in the text. [c] Calculated in μ_B at each temperature using the equation described in the text.

Table VII. Exchange Interactions in Dihydroxo- and Dialkoxo-Bridged Fe(III) Dimers

Complex	$-J$ (cm^{-1})[a]	Ref
$[Dipic(H_2O)FeOH]_2$	11.4	This work
$[Chel(H_2O)FeOH]_2 \cdot 4H_2O$	7.3	This work
$[(Pic)_2FeOH]_2$[b]	8	9
$[(Acac)FeOCH_3]_2$[c]	11	10
$[(DPM)_2FeOC_2H_5]_2$[d]	11	10
$[(DPM)_2FeO\text{-}n\text{-}C_3H_7]_2$	11	10
$[(DPM)_2FeOCH_3]_2$	8.5	10
$[(DPM)_2FeO\text{-}i\text{-}C_3H_7]_2$	10	10
$[Fe(SALPA)(SALPA\text{-}H)]_2$[e]	17	11a
$[Fe(SALPA)Cl]_2 \cdot C_6H_5CH_3$	17	11b

[a] Calculated from the $-2J\bar{S}_1\bar{S}_2$ model for $g = 2.00$ and TIP = 0. [b] Pic = pyridine-2-carboxylate. [c] Acac = anion of acetylacetone. [d] DPM = anion of dipivalomethane. [e] SALPA = dianion of Schiff's base from salicylaldehyde and 3-aminopropanol-1. The ferric ions in this dimeric complex are bridged by two propoxide groups.

were made to determine if either of the title complexes also exists as solution species.

The extent of antiferromagnetism exhibited by the title complexes is comparable to that reported for other Fe(III) complexes formulated as either $Fe_2(OH)_2^{4+}$ or $Fe_2(alkoxo)_2^{4+}$ species (Table VII). Of special interest are the recent crystallographic and magnetochemical studies of two dimeric Fe(III)–Schiff base complexes which have a $Fe_2(propoxide)_2^{4+}$ unit. In comparison to the title complexes, the $Fe_2(propoxide)_2^{4+}$ unit containing six-coordinate Fe(III)[11a] was found to have a longer Fe–Fe separation (3.217 (7) Å), comparable Fe–O distances ((1.988 (20), 1.972 (21); 1.970 (19), 1.919 (19) Å), and larger bridging angles (110.6 (9) and 108.2 (9)°). Magnetic susceptibility data obtained at 298, 195, and 77 K have been reported, but were not analyzed in detail. Our analysis of these data yielded a J value of -17 cm^{-1} for $g = 2.00$ and TIP = 0. The $Fe_2(propoxide)_2^{4+}$ unit containing five-coordinate Fe(III)[11b] was found to be structurally similar to the title complexes in regard to its Fe–Fe separation of 3.089 (6) Å and Fe–O bridging angle of 104.1 (6)°. Magnetochemical studies of this latter dimer as both a toluene solvate and an unsolvated species yielded J values of ca. -17 cm^{-1}. If the differences in the nature of the nonbridging ligands and in the coordination number of the Fe(III) ions may be ignored, then the systematic variation of magnetic behavior with bridging angle observed for a series of $Cu_2(OH)_2^{2+}$ species[8] is not exhibited by the two $Fe_2(OH)_2^{4+}$ and two $Fe_2(propoxide)_2^{4+}$ species described above. However, the number and nature of the exchange paths in the Cu(II) and Fe(III) dimers are different.[25] We are at this time unable to account for the observed variations in weak antiferromagnetic coupling (Table VII) that have been reported for various $Fe_2(OH)_2^{4+}$ and $Fe_2(alkoxo)_2^{4+}$ species. The effects of nonbridging ligands, Fe(III) coordination number, and Fe–O–Fe bridging angles do appear to be magnetically invisible in the more strongly coupled Fe_2O^{4+} units ($J = -95$ cm^{-1}).[28] The relative importance of such factors in the $Fe_2(OH)_2^{4+}$ and $Fe_2(alkoxo)_2^{4+}$ units remains to be established.

Consistent with theoretical expectations, magnetic coupling via the direct overlap of the Fe(III) d orbitals does not appear to be significant. As noted above, one of the $Fe_2(propoxide)_2^{4+}$ dimers has both a greater Fe–Fe separation and larger antiferromagnetism than were found for the title complexes. Still larger antiferromagnetism is exhibited by Fe_2O^{4+} dimers ($J \simeq -95$ cm^{-1})[28] and Fe_3O^{7+} trimers ($J \simeq -30$ cm^{-1})[29] where the Fe–Fe separations are 3.6 and 3.32 Å, respectively. Similar results have been observed for $Cr_2(OH)_2^{4+}$ species[30] and for various dimeric Cu(II) carboxylates.[31] It appears likely that "direct" spin–spin inter-

actions may be ignored for polynuclear Werner-type complexes of the first transition series metal ions.

Part of our incentive for a crystallographic study of both title complexes was to see if a structural basis for the observed difference in their magnetic behavior could be found. The electronic effects of substituting OH for H in the 4-pyridine position include an increased basicity of the ring nitrogen of Chel relative to that of Dipic.[32,33] On this basis, we had expected that the Fe-OH bond trans to the Fe-N bond in the Chel complex would be lengthened relative to the corresponding Fe-OH bond in the Dipic complex. Since the paths of exchange coupling should depend on the Fe-O bond distances in the bridges,[26] we had correctly predicted in advance the observed order of exchange coupling ($|J(\text{Dipic})| > |J(\text{Chel})|$). However, the Fe-OH and Fe-N bond distances and the Fe-*OH* bridging angles in both complexes were found to be identical within experimental error. Therefore, there is no structural support for the above chemical intuition. The substitution of an electron withdrawing group such as halogen, sulfone, etc., in the 4-position would allow a greater variation in the range of ligand basicities. Since crystallographic and preliminary magnetic studies ($J \simeq -95$ cm^{-1}) show the Fe(III) complex of the 4-chloro derivative to be a Fe_2O^{4+} system,[34] such a comparison may not be feasible for Fe(III). A more fruitful study may be possible for Cr(III) which has, relative to Fe(III), a larger affinity for N ligands. As noted above, both $[Chel(H_2O)CrOH]_2 \cdot 4H_2O$ and $[Dipic(H_2O)CrOH]_2$ have the $Cr_2(OH)_2^{4+}$ unit.

Finally, we consider the saga of the aquo dimer $[(H_2O)_4FeOH]_2^{4+}$ for which a J value of ca. -40 cm^{-1} has been estimated.[7] We see no compelling reasons why the aquo dimer should be either structurally or magnetically anomalous to the title complexes. Unfortunately, the unavailability of crystalline salts of the aquo dimer rules out definitive magnetic or structural studies. The mineral fibroferrite ($Fe_2O_3 \cdot 2SO_3 \cdot 11H_2O$) does bear a compositional similarity to $Al_2O_3 \cdot 2SO_3 \cdot 11H_2O$ which contains discrete $[(H_2O)_4AlOH]_2^{4+}$ ions (Al-OH-Al angle, 100.4°; Al···Al distance 2.86 Å).[35] However, the d spacings reported for the Al phase are different from those reported for fibroferrite[36] (and verified independently in this laboratory). The large and rapid water solubility of the Al phase in contrast to the poor solubility of the Fe phase furthermore suggests that fibroferrite consists of polymeric rather than dimeric units.

The title complexes constitute the best available models for the magnetic properties of the parent Fe(III) aquo dimer. If the geometries of the $Fe_2(OH)_2^{4+}$ units in these species are similar, their magnetic properties will very likely be comparable. Their geometrical equivalence may be approached in an indirect way by comparing the features of the $Al_2(OH)_2^{4+}$ units in the Chel and Dipic complexes with those reported for the $[(H_2O)_4Al(OH)_2Al(H_2O)_4]^{4+}$ species in the $Al_2O_3 \cdot 2SO_3 \cdot 11H_2O$ phase.[35]

A final comment concerns the magnetic properties at 77, 196, and 297 K which have been attributed to the Fe(III) aquo dimer as an adsorbed species on a sulfonate-type ion exchange resin.[7] The bulk susceptibility data (corrected for high-spin Fe(III) species) were accounted for by a J value for the dimer of -40 to -42 cm^{-1}. We have recently characterized a basic Fe(III) sulfate of composition $K_5[(H_2O)_3(SO_4)_6Fe_3O] \cdot 6H_2O$ which, in analogy to the well-known trimeric Fe(III) carboxylates, contains discrete $[(H_2O)_3(SO_4)_6Fe_3O]^{5-}$ units.[37] Antiferromagnetic coupling between the crystallographically equivalent Fe(III) ions is described well by the triangular cluster model for $J = -26.0$ cm^{-1}, $g = 2.00$, and TIP = 0. Similar species may also have formed on the sulfonate resin. Analysis of the trimer's magnetism by a model appropriate for a dimer yields, assuming $g = 2.00$ and TIP = 0, J values which systematically decrease from a value of -33.3 cm^{-1} at 299.6 K to -24.5 cm^{-1} at 96 K. The J value of ca. -40 cm^{-1} that has been attributed to the Fe(III) aquo dimer is inconsistent with those found for related Fe(III) dimers (Table VII) and cannot readily be rationalized by considering contributions from more highly condensed and antiferromagnetic species such as the trimeric Fe_3O^{7+} unit.

Acknowledgments. This research was supported by the Rutgers Computing Center (H.J.S., J.A.P.), the Rutgers Research Council (H.J.S.), and a Rutgers Biological Sciences Support Grant (H.J.S.). Magnetic measurements were made in the laboratory of Professor Harry B. Gray at the California Institute of Technology; H.J.S. thanks Professor Gray for his hospitality.

Supplementary Material Available: structure factor tables for $[Chel(H_2O)FeOH]_2 \cdot 4H_2O$ and $[Dipic(H_2O)FeOH]_2$ (16 pages). Ordering information is given on any current masthead page.

References and Notes

(1) Author to whom correspondence should be addressed.
(2) A. P. Sloan Fellow, 1971–1973.
(3) L. N. Mulay and P. W. Selwood, *J. Am. Chem. Soc.*, **77**, 2693 (1955).
(4) T. G. Spiro and P. Saltman, *Struct. Bonding (Berlin)*, **6**, 116 (1969).
(5) H. J. Schugar, C. Walling, R. B. Jones, and H. B. Gray, *J. Am. Chem. Soc.*, **89**, 3712 (1967).
(6) J. Mathe and E. Bakk-Mathe, *Rev. Roum. Chim.*, 11, 255 (1966).
(7) T. Nortia and E. Kontas, *Suom. Kemistil. B*, **44**, 406 (1971).
(8) K. T. McGregor, N. T. Watkins, D. L. Lewis, R. F. Drake, D. J. Hodgson, and W. E. Hatfield, *Inorg. Nucl. Chem. Lett.*, **9**, 423 (1973).
(9) H. J. Schugar, G. R. Rossman, and H. B. Gray, *J. Am. Chem. Soc.*, **91**, 4564 (1969).
(10) C. S. Wu, G. R. Rossman, H. B. Gray, G. S. Hammond, and H. J. Schugar, *Inorg. Chem.*, **11**, 990 (1972).
(11) (a) J. A. Bertrand and P. G. Eller, *Inorg. Chem.*, **13**, 927 (1974); published susceptibility data at 298, 195, and 77 K correspond to $J = -17$ cm^{-1} for $g = 2.00$ and TIP = 0. (b) J. A. Bertrand, J. L. Breece, and P. G. Eller, *ibid.*, **13**, 125 (1974).
(12) S. P. Gag, Q. Fernando, and H. Fraser, *Inorg. Chem.*, **1**, 887 (1962).
(13) C. Ou, W. Borowski, J. A. Potenza, and H. J. Schugar, to be submitted for publication. $[Dipic(H_2O)CrOH]_2$ crystallizes in the monoclinic space group $C_{2/m}$ with $Z = 2$, $a = 12.366$ (5) Å, $b = 10.847$ (7) Å, $c = 7.162$ (4) Å, $\beta = 117.51$ (3)°, and $d_{obsd} = 1.95$ (1) g/cm^3. R_F currently is 4.9%.
(14) H. J. Schugar, G. R. Rossman, C. G. Barraclough, and H. B. Gray, *J. Am. Chem. Soc.*, **94**, 2683 (1972).
(15) See A. Earnshaw, "Magnetochemistry", Academic Press, New York, N.Y., 1969, p 77.
(16) In addition to local programs for the IBM 360/67 computer, local modifications of the following programs were employed: Zalkin's FORDAP Fourier program; Johnson's ORTEP II thermal ellipsoid plotting program; Busing, Martin, and Levy's ORFFE error function and ORFLS least-squares programs.
(17) D. T. Cromer and J. T. Waber, *Acta Crystallogr.*, **18**, 104 (1965).
(18) International Tables for X-Ray Crystallography, Vol. III, Kynoch Press, Birmingham, England, 1962, p 201–213.
(19) The analysis of variance was performed using the program NANOVA obtained from Professor I. Bernal; see J. S. Ricci, Jr., C. A. Eggers, and I. Bernal, *Inorg. Chim. Acta*, **6**, 97 (1972).
(20) See paragraph at end of paper regarding supplementary material.
(21) R. D. Shannon and C. T. Prewitt, *Acta Crystallogr., Sect. B*, **25**, 925 (1969).
(22) F. Takusagawa, K. Hirotsu, and A. Shimada, *Bull. Chem. Soc. Jpn.*, **46**, 2020 (1973), and references therein.
(23) B. R. Penfold, *Acta Crystallogr.*, **6**, 591 (1953).
(24) D. Powers, G. R. Rossman, H. J. Schugar, and H. B. Gray, *J. Solid State Chem.*, **13**, 1 (1975).
(25) J. S. Griffith, *Struct. Bonding (Berlin)*, **10**, 87 (1972).
(26) A. P. Ginsberg, *Inorg. Chim. Acta Rev.*, **5**, 45 (1971), and references therin.
(27) von G. Anderegg, *Helv. Chim. Acta*, **43**, 1530 (1960).
(28) K. S. Murray, *Coord. Chem. Rev.*, **12**, 1 (1974).
(29) E. M. Holt, S. L. Holt, W. F. Tucker, R. O. Asplund, and K. J. Watson, *J. Am. Chem. Soc.*, **96**, 2621 (1974).
(30) J. T. Veal, W. E. Hatfield, and D. J. Hodgson, *Acta Crystallogr., Sect. B*, **29**, 12 (1973).
(31) J. A. Moreland and R. J. Doedens, *J. Chem. Soc., Chem. Commun.*, 28 (1974).
(32) von E. Blasius and B. Brozio, *Ber. Bunsenges. Phys. Chem.*, **68**, 52 (1964).

(33) A. Albert in "Physical Methods in Heterocyclic Chemistry", Vol. III, A. R. Katritzky, Ed., Academic Press, New York, N.Y., 1971, Chapter 9.
(34) C. Ou, D. Powers, J. A. Potenza, and H. J. Schugar, unpublished results.
(35) G. Johansson, *Acta Chem. Scand.*, **16**, 403 (1962).
(36) F. Cesbron, *Bull. Soc. Fr. Mineral. Cristallogr.*, **87**, 125 (1964); *Struct. Rep.*, **20**, 343 (1956).
(37) J. A. Thich, B. Vasiliou, D. Mastropaolo, D. Powers, J. A. Potenza, and H. J. Schugar, to be submitted for publication.

Acid–Base Properties and Gas-Phase Ion Chemistry of $(CH_3)_3B$

M. K. Murphy[1a] and J. L. Beauchamp*[1b]

Contribution No. 5117 from the Arthur Amos Noyes Laboratory of Chemical Physics, California Institute of Technology, Pasadena, California 91125. *Received May 28, 1975*

Abstract: The ion-molecule reactions of trimethylborane, $(CH_3)_3B$, both alone and in mixtures with other molecules, have been investigated by ion cyclotron resonance spectroscopy. Reaction pathways, product distributions, and reaction rate constants have been determined for a variety of reactions involving both positive and negative ions. Where possible thermochemical data have been obtained, including the gas-phase Brönsted acidity, $PA[(CH_3)_2B{=}CH_2^-] = 365 \pm 5$ kcal/mol. Attempts to determine the Brönsted base strength were frustrated by failure to observe protonated $(CH_3)_3B$. Exothermic proton transfer reactions lead exclusively to the formation of $(CH_3)_2B^+$ and CH_4. The thermoneutral CH_3^- transfer reaction $(CH_3)_2{}^{10}B^+ + (CH_3)_3{}^{11}B \rightleftharpoons (CH_3)_3{}^{10}B + (CH_3)_2{}^{11}B^+$ is observed to be rapid with $k_f = k_r = 2.6 \times 10^{-10}$ cm^3 molecule^{-1} sec^{-1}. Transfer of D^- and F^- from appropriate reagent anions to $(CH_3)_3B$ produces the four-coordinate anions $(CH_3)_3BD^-$ and $(CH_3)_3BF^-$, which are discussed in light of the electron pair acceptor capabilities of the vacant B 2p valence orbital in the neutral. Photoionization efficiency curves for ions generated in $(CH_3)_3B$ between 9.7 and 10.8 eV photon energies have been obtained, yielding the adiabatic $IP[(CH_3)_3B] = 10.01 \pm 0.02$ eV, the fragmentation threshold, $AP[(CH_3)_2B^+] = 10.35 \pm 0.05$ eV, and the B–CH_3 bond dissociation energy in the parent radical ion, $D[(CH_3)_2B^+{-}CH_3] = 7.8 \pm 1$ kcal/mol.

Ion cyclotron resonance (ICR) mass spectrometry provides a tool uniquely suited to the detailed study of ion-molecule chemistry in the gas phase, in the absence of complicating solvation phenomena. Recently reported from this laboratory have been the reactions of Li^+, NO^+, and carbonium ions exemplary of their behavior as Lewis acids.[2-7] Studies of relative Lewis acidities of carbonium ions toward the reference bases H^-, F^-, and Br^- have been used to measure relative carbonium ion stabilities in the gas phase.[4-7] A natural extension of this work is the determination of the relative Lewis acidities of various neutral acceptors toward these same Lewis bases. Recently reported gas phase studies along these lines have discussed the relative binding energies of F^- and Cl^- to hydrogen halides (HX where X = F, Cl, Br),[8] compounds possessing the hydroxyl functional group (including water, several alcohols, and carboxylic acids)[9] and a variety of inorganic Lewis acids.[10]

As part of an extensive investigation of the group 3 Lewis acids MX_3 (where M = B, Al, ···; X = H, alkyl, halogen) in this laboratory, this report describes ICR and photoionization mass spectrometry (PIMS) studies of the thermochemical properties and reactions of positive and negative ions derived from trimethylborane, $(CH_3)_3B$. This molecule, unlike many group 3 Lewis acids, exists as a trigonal planar monomer in the gas phase at room temperature.[11] As such, an investigation of its ion chemistry may provide insights into the effects of valence shell electron deficiency, resulting from the presence of a vacant B 2p orbital in the neutral, on ionic reactivity and stability.

Investigation of Lewis acidity of boron compounds has been extensive, but has dealt largely with neutral adducts formed between acids BX_3 and various *n*-donor bases (e.g., amines, phosphines).[12,13] Previous gas phase studies of the ion chemistry of boron containing compounds have considered boron hydrides,[14] tri-*n*-butylborane,[15] boron halides,[10] and borazine.[16] Unlike $(CH_3)_3B$, interaction of boron atoms via multicenter bonding present in even the simplest boron hydrides complicates efforts to elucidate the effects of a single vacant B 2p orbital.[17] Such is also the case in the monomeric boron trihalides, where the B 2p orbital is extensively involved in dative π bonding to the halide substituents.[18]

Previous investigations of ions derived from $(CH_3)_3B$ utilizing conventional electron impact mass spectrometry deal only with positive ions.[19-22] These studies of $(CH_3)_3B$ entail ionization (IP) and appearance potential (AP) measurements, correlation of fragmentation patterns for structural determination, and the effects of isotopic substitution ($^{1,2}H$, $^{10,11}B$, $^{12,13}C$) on fragmentation patterns.[20-22] Thermochemical data on ions containing boron are limited, with considerable disagreement among reported values (Table I).

Experimental Section

The instrumentation and techniques associated with ICR spectrometry are described in detail elsewhere.[23,24] In studies reported here, both a modified Varian V-5900 spectrometer and a larger, high field instrument, constructed in the laboratory are employed.[24] Gas mixtures utilized are prepared directly in the ICR cell by admission of the appropriate sample components through separate variable leak valves in a parallel inlet manifold. Absolute gas pressures are determined using a Schulz-Phelps ionization gauge, adjacent to the ICR cell, calibrated searately for each component against an MKS Baratron Model 90H1-E capacitance manometer.[5] A linear calibration of Baratron pressure vs. ionization gauge current affords pressure determinations over a range of 10^{-7} to 10^{-4} Torr. The overall accuracy in pressure measurement for these studies is estimated to be ±20%, and represents the major source of error in reported reaction rate constants.

Photoionization measurements of $(CH_3)_3B$ utilize the Caltech-JPL facility, which has been previously described.[25] Pertinent operating conditions include: source temperature, ambient (22°C); ion source sample pressure, 1.6×10^{-4} Torr; resolution, 1 Å; repeller field, 0.1 V/cm; ion energy for mass analysis, 20 eV. The hydrogen many-line spectrum is utilized as the photon source for the wavelength range studied (1290–1140 Å). Photon intensities are